Supplementary Information for

Plasmonic Mesoporous AuAg Nanospheres with Controllable Nanostructures

Hao Lv,[a] Lizhi Sun,[b] Ji Feng,[c] Jongbeom Na,[d,e] Dongdong Xu,[b] Yusuke Yamauchi,[d,f] and Ben Liu[*,a,b]

[a]College of Chemistry, Sichuan University, Chengdu 610064, China

[b]Jiangsu Key Laboratory of New Power Batteries, Jiangsu Collaborative Innovation Center of Biomedical Functional Materials, School of Chemistry and Materials Science, Nanjing Normal University, Nanjing 210023, China. E-mail: ben.liu@njnu.edu.cn

[c]Department of Chemistry, University of California, Riverside, California 92521, United States

[d]School of Chemical Engineering and Australian Institute for Bioengineering and Nanotechnology (AIBN), The University of Queensland, Brisbane, QLD 4072, Australia

[e]International Center for Materials Nanoarchitectonics (WPI-MANA), National Institute for Materials Science (NIMS), 1-1 Namiki, Tsukuba 305-0044, Japan

[f]Department of Plant & Environmental New Resources, Kyung Hee University, 1732 Deogyeong-daero, Giheung-gu, Yongin-si, Gyeonggi-do 17104, South Korea

Table of Contents

1. Chemicals and Materials

Chloroauric acid ($HAuCl_4$) and silver nitrate ($AgNO_3$) was purchased from Alfa Aesar. L-ascorbic acid, hydrazine hydrate (N_2H_4, 50%), sodium borohydride ($NaBH_4$), hydrochloric acid, and sodium hydroxide were obtained from Sinopharm Chemical Reagent Co. Ltd. (Shanghai). *N, N*-dimethyldocosylamine ($C_{22}H_{45}N(CH_3)_2$) was purchased from Heowns Opde Technologies (Tianjin). 3-Chloro-1-propanethiol (Cl-C_3H_6-SH) was obtained from Sigma-Aldrich. Amphiphilic C_{22}N-SH was synthesized based on our previous method (*Chem. Sci.* **2019**, *10*, 6423). All the reagents were of analytical reagent grade and used without further purification.

2. Synthesis of mesoporous AuAg (mesoAuAg), hollow mesorpous AuAg (h-mesoAuAg), and core-shell Ag-mesoporous Au (Ag@mesoAu)

Well-alloyed mesoAuAg nanospheres were synthesized in an aqueous solution with C_{22}N-SH as a surfactant template, $HAuCl_4$ and $AgNO_3$ as metal precursors, and N_2H_4 as a reducing agent. In a typical synthesis, 30 mg of C_{22}N-SH was dissolved in 5 mL of water. After 30 min, 0.36 mL of 0.1 M NaOH, 0.8 mL of 10 mM $HAuCl_4$ and 0.2 mL of 10 mM $AgNO_3$ solution were consecutively injected. Then, after kept at 25 ^oC undisturbed for 10 min, 6.4 mL of N_2H_4 was injected into above solution. Then, the products were collected by washing with H_2SO_4 and H_2O_2 (3/1 by volume) for three times and with H_2O for six times.

h-mesoAuAg nanospheres were synthesized with the same procedures for mesoAuAg, but with different surfactant concentration. Typically, 45 mg of C_{22}N-SH was dissolved in 5 mL of water. After 30 min, 0.36 mL of 0.1 M NaOH, 0.8 mL of 10 mM $HAuCl_4$ and 0.2 mL of 10 mM $AgNO_3$ solution were consecutively injected. Then, after kept at 25 ^oC undisturbed for 10 min, 6.4 mL of N_2H_4 was injected into the above solution. Then, the products were collected by washing with H_2SO_4 and H_2O_2 (3/1 by volume) for three times and with H_2O for six times.

Core-shell Ag-mesoAu nanospheres were synthesized with the same procedures for h-mesoAuAg, but with different reaction temperature. Typically, 45 mg of C_{22}N-SH was dissolved in 5 mL of water. After 30 min, 0.36 mL of 0.1 M NaOH, 0.8 mL of 10 mM $HAuCl_4$ and 0.2 mL of 10 mM $AgNO_3$ solution were consecutively injected. Then, the solution was heated to 45 ^oC, and kept undisturbed for 10 min. After injecting 6.4 mL of N_2H_4 into the above solution, the products were collected by washing with H_2SO_4 and H_2O_2 (3/1 by volume) for three times and with H_2O for six times.

Au-4 NPs were synthesized according to previous reports (*Chem. Sci.* **2019**, *10*, 6423; *Nat. Commun.* **2014**, *5*, 4947).

3. Electrochemical methanol oxidation reaction (MOR)

Electrocatalytic tests were performed on the CHI 750E electrochemical analyzer at 25 ^{o}C, based on our previous work (*Chem. Sci.* **2019**, *10*, 6423). A three-electrodes system was used for all electrochemical tests, which consisted of a carbon rod as the counter electrode, a silver/silver chloride electrode (SCE) as the reference electrode, and the nanocatalysts coated onto glassy carbon electrode (GCE, 0.07065 cm^2) as the working electrode. The potentials used in this work were reported with respect to the Ag/AgCl electrode (SCE). The catalysts inks were prepared as followed: 1 mg of nanocatalysts and 4 mg of Vulcan XC-72 were dissolved in 1 mL of co-solvents of ethanol and water (4/1 by vol.); after the sonication for 30 min, 50 µL of Nafion was injected in the ink with another 30 min sonication. Then, 3.0 µL of the catalysts ink was dropped on the GCE electrode and dried at room temperature for electrocatalytic investigations. The CVs and ECSAs were obtained in N_2-saturated 0.5 M H_2SO_4, while electrocatalytic MOR performances were performed in 0.5 M KOH and 2.0 M methanol. Electrochemical *i-t* chronoamperograms of all the nanocatalysts were collected at their corresponding peak oxidation potentials for 2000 seconds.

4. Characterizations

Transmission electron microscope (TEM) observations were performed with a JEOL JEM-2100 microscope operated at 200 kV (Cs 0.5 mm, point resolution 1.9 Å). High-angle annular dark-field scanning STEM was taken on JEOL JEM-2100F microscope that are equipped with STEM and EDS detectors for elemental mapping analysis. TEM and STEM samples were prepared by casting a suspension of the samples on a carbon-coated copper grid (300 mesh). TEM samples of mesoAuAg intermediates were prepared by quickly dipping TEM grids into the reaction solution under different reduction times (5 s, 15 s, 30 s, and 120 s) and taking it out immediately. X-ray diffraction (XRD) patterns were recorded on powder samples using a D/max 2500 VL/PC diffractometer (Japan) equipped with graphite-monochromatized Cu Kα radiation. X-ray photoelectron spectra (XPS) were performed on a scanning X-ray microprobe (Thermo ESCALAB 250Xi) that uses Al Kα radiation. The binding energy of the C 1s peak (284.8 eV) was employed as a standard to calibrate the binding energies of other elements (Au and Ag et al.). Ultraviolet-visible (UV-vis) absorption spectroscopy was obtained on Shimadzu UV-2450 ultraviolet-visible spectrophotometer. Inductively coupled plasma mass spectrometry (ICP-MS) was recorded on a NexION 350D.

5. Supplementary Figures

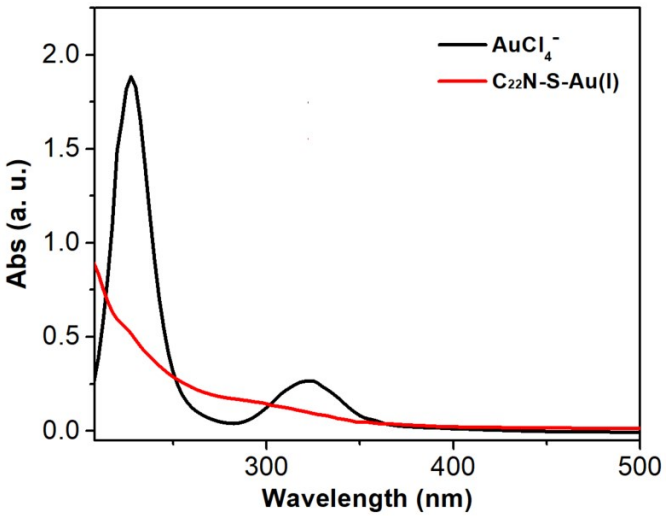

Fig. S1 UV-vis spectra of $HAuCl_4$ and $C_{22}N$-S-Au(I).

Notes for Fig. S1: The disappearance of characteristic signals ascribed to $AuCl_4^-$ after mixing with $C_{22}N$-SH indicates the self-reduction of $AuCl_4^-$ into Au(I) and the formation of polymeric $C_{22}N$-S-Au(I) intermediates.

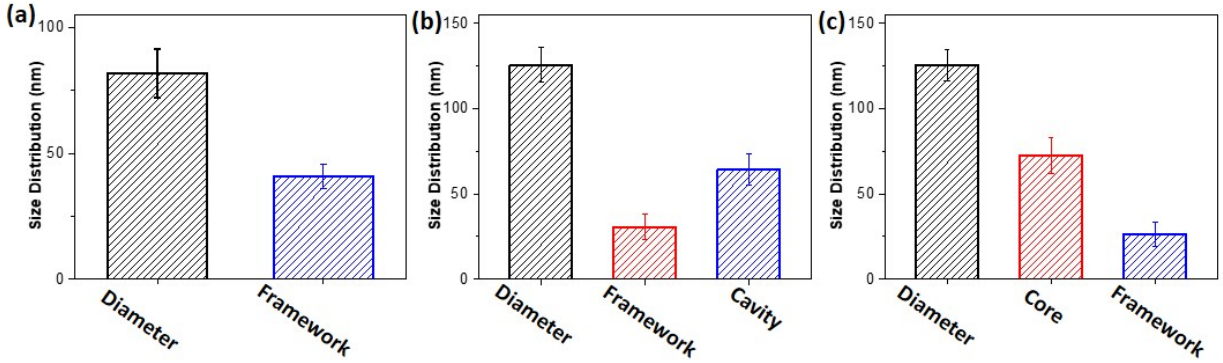

Fig. S2 Size distributions of well-alloyed mesoAuAg, h-mesoAuAg and core-shell Ag@mesoAu nanospheres.

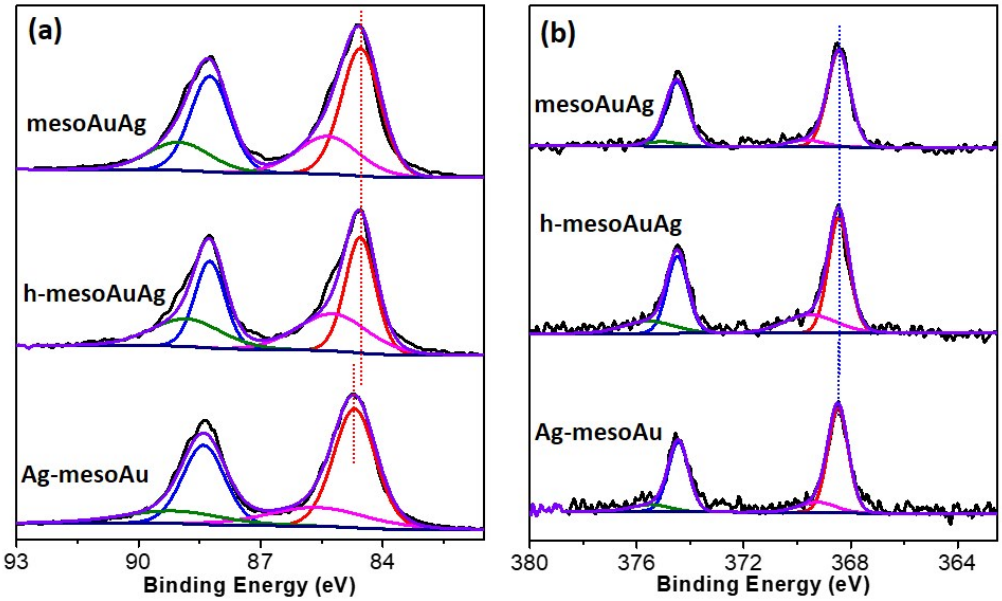

Fig. S3 High-resolution XPS (a) Au 4f and (b) Ag 3d spectra of well-alloyed mesoAuAg, h-mesoAuAg, and core-shell Ag-mesoAu nanospheres.

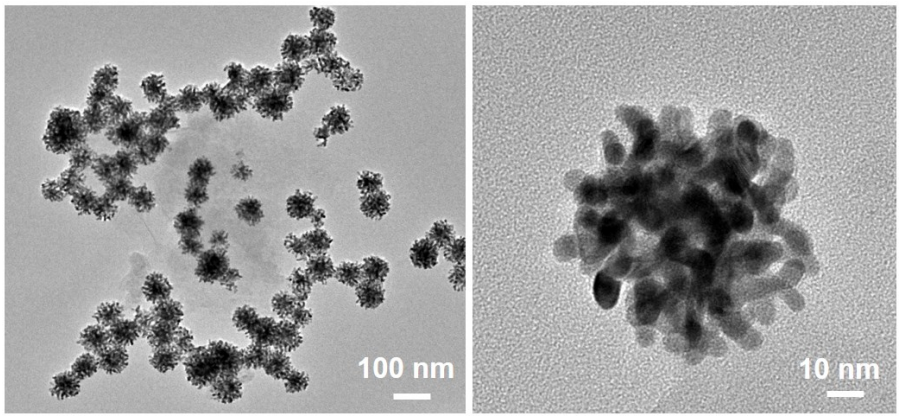

Fig. S4 TEM images of mesoAu nanospheres synthesized with $AuCl_4^-$ as the sole metal precursor.

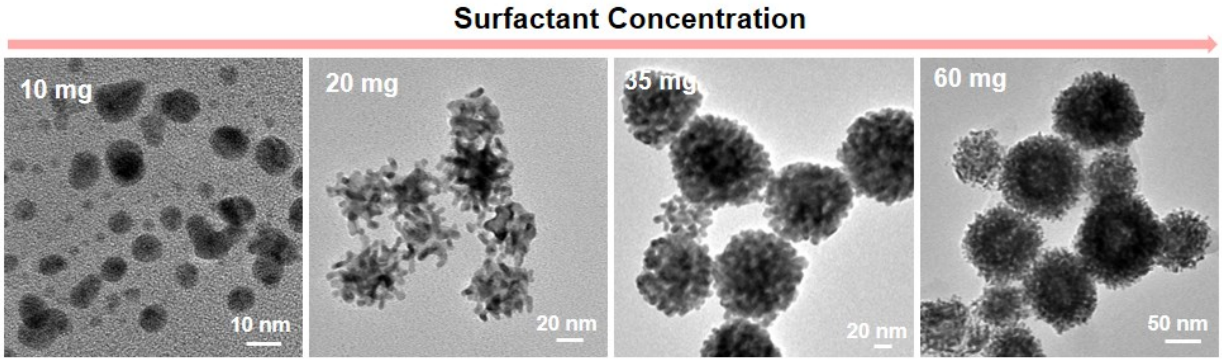

Fig. S5 The effect of surfactant concentrations in engineering nanostructures of mesoAuAg nanospheres.

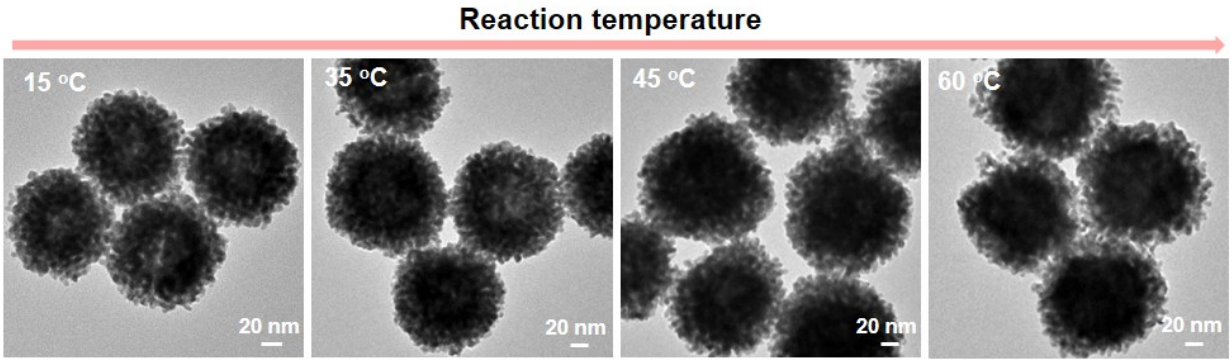

Fig. S6 The effect of reaction temperatures in engineering nanostructures of mesoAuAg nanospheres.

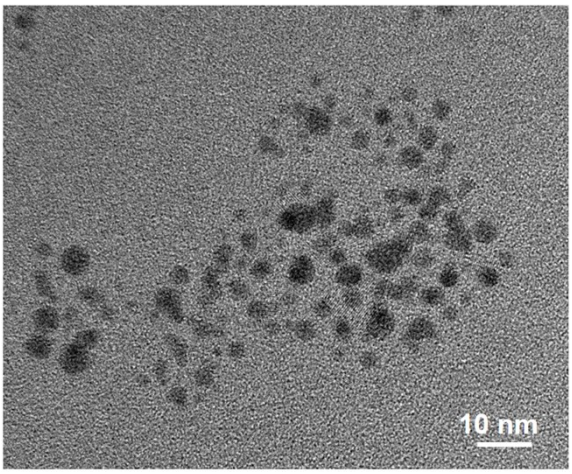

Fig. S7 TEM image of Au-4.

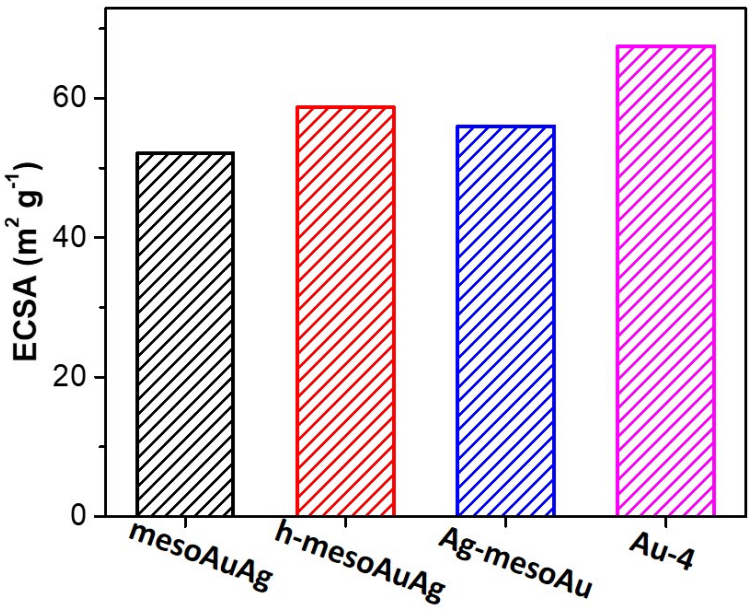

Fig. S8 The ECSA values of mesoAuAg, h-mesoAuAg, Ag-mesoAuAg, and Au-4.

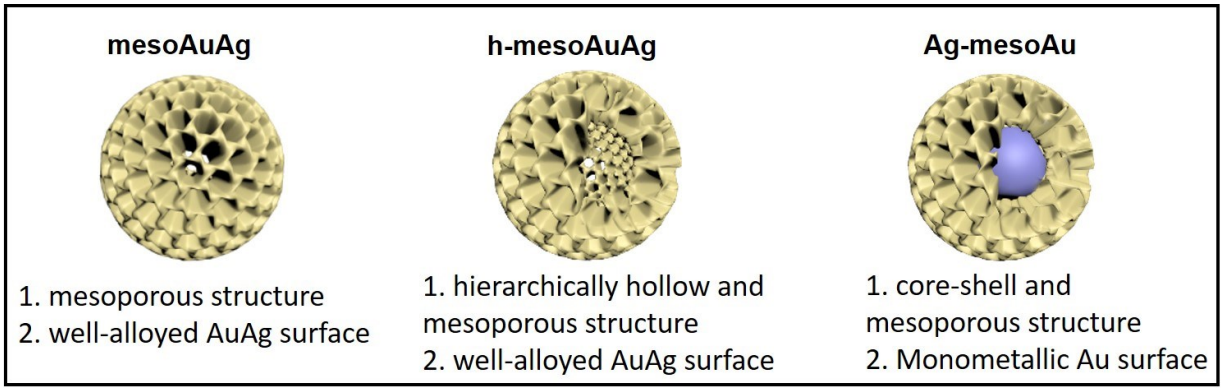

Fig. S9 Structural and compositional features of well-alloyed mesoAuAg, h-mesoAuAg and core-shell Ag-mesoAu.

Notes for **Fig. S9**: Based on the structural and composition features, we attributed the better catalytic activity of h-mesoAuAg to its hierarchically hollow cavity and interconnected mesoporous framework that exposed the highdensity low-coordinated sites and accelerated the mass transport. In contrast, the catalytic sites of mesoAuAg and Ag-mesoAu, especially in the centers, may be partially blocked during the electrocatalysis. Meanwhile, Ag-mesoAu is composed almost completely of monometallic Au sites on the surface, disabling the compositional synergy of the bimetallic AuAg alloys.

6. Supplementary Tables

Table S1. Elemental compositions of mesoAuAg with different nanostructures collected with ICP-MS.

Samples	mesoAuAg	h-mesoAuAg	Ag-mesoAu
Au/Ag ratios	81.2:18.8	79.9:20.1	80.4:19.6

Notes for Table S1: The feed ratios of Au/Ag for the syntheses of mesoAuAg with different nanostructures are 8:2. The final Au/Ag ratios in different mesoAuAg are ~ 80:20, indicating complete reduction and crystalline during the synthesis.

Table S2. Summarizations of the activities of Au-based catalysts in the electrocatalytic MOR.

Nanocatalysts	Measurement Conditions			Mass activity ($\mu A\ \mu g^{-1}$)	Ref.
	Scan rate ($mV\ s^{-1}$)	CH_3OH con. (M)	KOH con. (M)		
h-mesoAuAg	20	2.0	0.5	42.9	This work
mesoAuAg	20	2.0	0.5	34.94	This work
Ag@mesoAu	20	2.0	0.5	29.35223	This work
Mesoporous Au nanospheres	20	2.0	0.5	29.9	*Chem. Sci.* **2019**, *10*, 6423
Nanoporous Au	10	1.0	0.5	28	*ACS Appl. Mater. Interface* **2016**, *8*, 23920
Nanoporous Au nanobowls	10	2.0	0.5	26	*Small*, **2016**, *12*, 4531
Au NPs on carbon	50	1.0	0.1	~21	*Electrochim. Acta* **2013**, *94*, 159
Au nanoparticles	50	1.0	1.0	~20	*Electrochim. Acta* **2006**, *52*, 1662
Nanoporous Au NPs	20	2.0	0.5	16.8	*Nat. Commun.* **2014**, *5*, 4947
mesoAu network	10	2.0	0.5	13.1	*Nat. Commun.* **2018**, *9*, 521